

Scanning capacitance microscopy of ErAs nanoparticles embedded in GaAs pn junctions

K. W. Park, H. P. Nair, A. M. Crook, S. R. Bank, and E. T. Yu^{a)}

Microelectronics Research Center, University of Texas at Austin, 10100 Burnet Rd., Austin, Texas 78758, USA

(Received 13 May 2011; accepted 2 September 2011; published online 29 September 2011)

Scanning capacitance microscopy is used to characterize the electronic properties of ErAs nanoparticles embedded in GaAs pn junctions grown by molecular beam epitaxy. Voltage-dependent capacitance images reveal localized variations in subsurface electronic structure near buried ErAs nanoparticles at lateral length scales of 20-30 nm. Numerical modeling indicates that these variations arise from inhomogeneities in charge modulation due to Fermi level pinning behavior associated with the embedded ErAs nanoparticles. Statistical analysis of image data yields an average particle radius of 6-8 nm—well below the direct resolution limit in scanning capacitance microscopy but discernible via analysis of patterns in nanoscale capacitance images.

© 2011 American Institute of Physics. [doi:10.1063/1.3644144]

Rare earth monpnictide (RE-V) alloys embedded in III-V compound semiconductors are currently the subject of intense research for applications such as multijunction tandem solar cells,¹ thermoelectric devices,^{2,3} and ultrafast optical devices.⁴ However, more detailed understanding of the electronic properties of RE-V nanoparticles in III-V semiconductors is required for further improvement in electrical properties and performance in device applications.

In this letter, we describe nanometer scale electronic characterization of GaAs p⁺/n⁺ junctions with embedded semimetallic ErAs nanoparticles using scanning capacitance microscopy (SCM). SCM has been widely used to characterize local surface and near-surface electronic structure for III-V semiconductors,⁵⁻⁷ providing images of nanoscale carrier modulation via bias voltages applied to a highly conductive proximal probe tip. The lateral spatial resolution arises from the use of a scanning probe tip, and vertical resolution is provided by the dependence of the carrier depletion depth on bias voltage. Our studies reveal lateral variations in charge accumulation behavior in the vicinity of buried ErAs nanoparticles, which we attribute to local Fermi level pinning by the embedded ErAs nanoparticles. Furthermore, we show that statistical analysis of spatial variations in capacitance enables ErAs nanoparticle sizes to be deduced, despite their being well below the resolution limit of direct scanning capacitance imaging.

The GaAs p⁺/n⁺ junction samples employed in this study were grown in a Varian GEN II solid-source molecular beam epitaxy (MBE) machine. The sample structures consisted of (100) n-GaAs substrates upon which were deposited 200 nm n⁺ GaAs (Si-doped, $n \sim 5 \times 10^{18} \text{ cm}^{-3}$), an ErAs nanoparticle layer, and a 1.5 nm p⁺ GaAs (Be-doped, $p \sim 5 \times 10^{19} \text{ cm}^{-3}$) capping layer; all layers were grown at 515 °C. For the ErAs nanoparticle layer, 1 monolayer (ML) of ErAs was deposited on the n⁺ GaAs surface. Since ErAs does not wet the GaAs surface, this results in growth of ErAs islands ~ 3 -4 ML thickness, covering approximately 25%-33% of the GaAs surface.^{8,9} The uncovered areas of the n⁺ GaAs surface serve as seeds for overgrowth of 1.5 nm p-type GaAs capping layers

on the ErAs islands.⁹ The rms surface roughness measured by atomic force microscopy (AFM) was ~ 0.33 nm, about half of the estimated surface roughness for the case of exposed ErAs nanoparticles, suggesting that the ErAs nanoparticles are fully covered by the 1.5 nm GaAs capping layer. This conclusion is also supported by comparison of SCM data from control samples containing no ErAs with that from samples with ErAs nanoparticle layers. A Veeco ICON atomic force microscope with a scanning capacitance measurement module was used to obtain surface topography and SCM images simultaneously at room temperature and in ambient atmosphere. Silicon probe tips coated with boron-doped diamond were used for proximal probing. Measurements were recorded with inverted polarity, which was found to provide optimal sensitivity in the SCM measurements. A schematic diagram of the samples used in this study and electrical connections for the SCM measurements is shown in Fig. 1.

Figure 2 shows surface topography and scanning capacitance images obtained for dc bias voltages ranging from -2 V to 0 V with 0.5 V amplitude, 90 kHz ac voltage modulation; SCM images from a reference sample consisting of a GaAs pn junction without ErAs nanoparticles are also shown. All bias voltages are specified as the potential of the probe tip relative to the sample. A strong dependence of SCM image contrast on dc bias voltage for the sample with ErAs nanoparticles is evident. For the sample with ErAs nanoparticles, the SCM images shown were obtained from two different measurement locations: -2.0 V and -1.5 V at one location, -1.0 V to 0.0 V at the other. Contrast arises in each SCM image which, on the basis of numerical modeling described below, we associate with varying local subsurface ErAs content within the sample region directly below the probe tip. The rectangles and circles in Fig. 2 mark identical locations in each imaged area, and denote locations with high and low local subsurface ErAs content, respectively.

Simulations using a one-dimensional numerical Poisson solver¹⁰ were employed to assess the influence of local subsurface ErAs content on the SCM signals. The ErAs nanoparticle layer was modeled as a planar ErAs layer with the Fermi level ~ 0.84 eV below the GaAs conduction-band

^{a)}Electronic mail: ety@ece.utexas.edu.

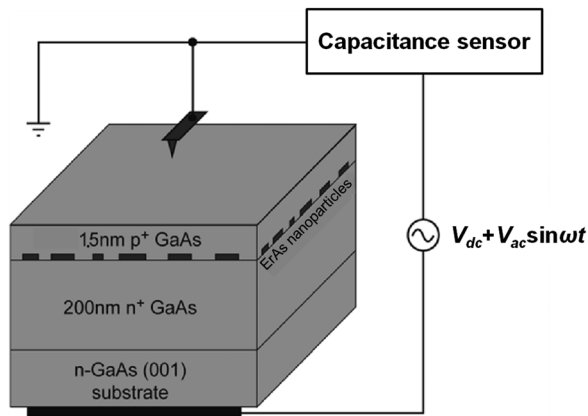


FIG. 1. Schematic diagram of GaAs pn junction with ErAs nanoparticles and of scanning capacitance measurement geometry and electrical connections.

edge.^{11,12} To simulate variations in local subsurface ErAs content, variable densities of states in the ErAs layer were employed, with effective masses of $0.32m_e$, $0.235m_e$, and $0.066m_e$ for electrons, heavy holes, and light holes¹³ corresponding to complete ErAs coverage. The degeneracy associated with the three equivalent X-point conduction band minima is also included.¹³ The electronic density of states in the ErAs layer is taken to be proportional to the fractional ErAs coverage at the pn junction.

Figure 3(a) shows simulated plots of $-dC/dV$ as a function of bias voltage for fractional ErAs coverages of 10%, 25%, 50%, and 60%; as noted above, based on epitaxial growth conditions we expect an average ErAs coverage of 25%-33% at the pn junction in our samples. Since the SCM

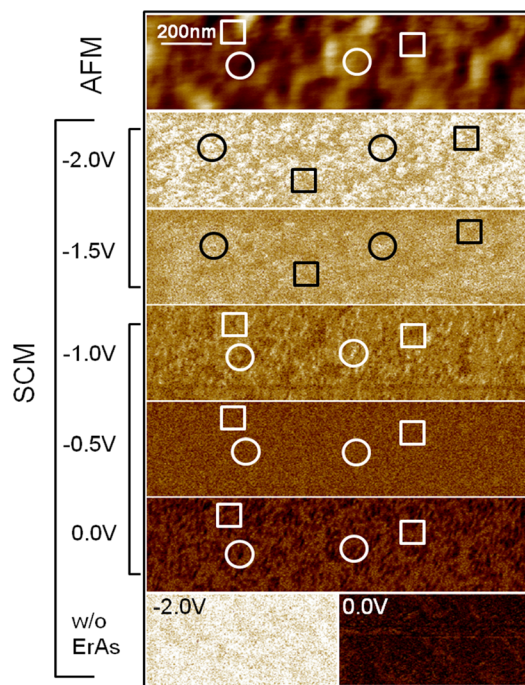


FIG. 2. (Color online) AFM surface topograph and SCM images for applied dc bias voltages ranging from -2.0V to 0V . SCM images obtained from identical areas are indicated by the brackets immediately to the left of the images. The AFM topograph was obtained simultaneously with the SCM image at 0V . The centers of rectangles and circles indicate locations in each image corresponding to high and low subsurface ErAs content, respectively. The bottom SCM images were taken from a GaAs-only reference sample at -2.0V and 0V . All SCM images are shown using the same signal-level scale.

signal is proportional to $-dC/dV$, we deduce from the simulations that regions with high subsurface ErAs coverage should exhibit SCM signal levels close to zero over a broad range of bias voltages. In contrast, areas with low ErAs coverage at the pn junction should exhibit a substantial voltage dependence of the SCM signal. The simulation results suggest inversion in image contrast between ErAs-rich and ErAs-poor regions should occur near -0.5V . Figure 3(b) shows SCM signal levels as a function of voltage extracted from the SCM images shown in Fig. 2, with each curve being at a location interpreted, based on the trends revealed in the numerical simulations, to correspond to either low or high subsurface ErAs content. The expected inversion in contrast is observed directly in the series of images, obtained from one location, spanning bias voltages from -1.0V to 0.0V . At more negative bias voltages of -1.5V and -2.0V , the signal levels observed are consistent with those between -1.0V and 0.0V . The SCM signal levels observed for the GaAs reference sample are also seen to be in excellent accord with these trends. The explicit observation of inversion in contrast and the trend in measured SCM signal levels across multiple locations and samples provide strong support for the interpretation that the contrast observed in the SCM images is associated with local nanoscale variations in the subsurface ErAs content. The observed charge modulation behavior can be explained with energy band diagrams computed for structures with high (60%) and low (10%) ErAs content, as shown in Figure 3(c). For high ErAs content, the large density of states associated with the ErAs nanoparticle layer causes most of the charge modulation to occur within the ErAs nanoparticles, leading to capacitance nearly independent of bias voltage. For low ErAs content, substantial charge modulation occurs at the n-GaAs depletion layer edge as well, leading to a bias-dependent capacitance. Additional simulations have shown that variations in GaAs capping

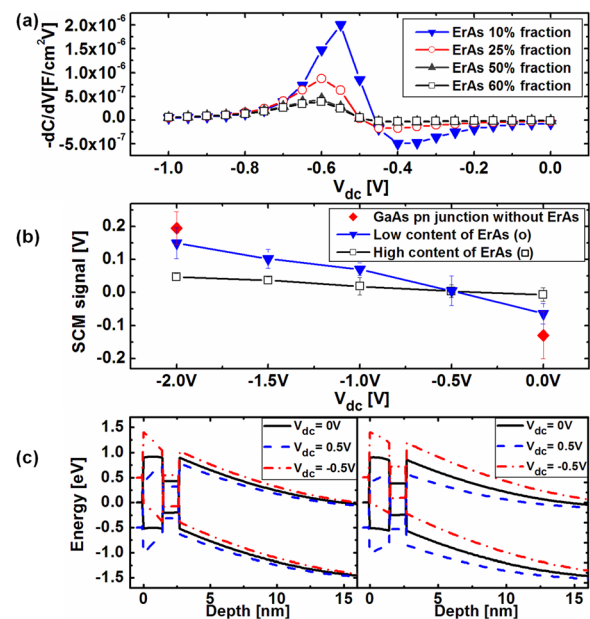


FIG. 3. (Color online) (a) Simulated values for $-dC/dV$ as a function of local subsurface ErAs content. (b) SCM signal levels extracted from the images shown in Fig. 2. (c) Energy band diagrams for the GaAs pn junction with ErAs nanoparticle fractional coverages of 60% (left) and 10% (right), under applied dc voltages of -0.5V , 0V , and $+0.5\text{V}$.

layer thickness in the range of 0.5-1.5 nm should have a much smaller effect on the observed SCM signal levels.

A statistical analysis of spatial inhomogeneity in the SCM image contrast shown in Fig. 2 provides information about ErAs nanoparticle size distributions, even for sizes well below the SCM resolution limit of ~ 30 -50 nm, which is governed primarily by the probe tip size. We define a threshold SCM signal level such that the fraction of points in the image below (for the SCM images at -1.0 V to -2.0 V) or above (for the SCM image at 0 V) this threshold level corresponds to the fractional surface coverage, f , expected based on epitaxial growth conditions. In this case, f is ~ 0.28 . The images are then divided into $40\text{ nm} \times 40\text{ nm}$ areas, corresponding approximately to the effective area probed in each SCM signal measurement. For each area, the fraction of points with signal levels below (or above) the threshold level is computed and taken as a measure of the fractional ErAs coverage within that area. This approach provides an estimate of the spatial dependence of ErAs coverage fraction as probed by SCM without requiring exact knowledge of the functional mapping of local ErAs coverage to SCM signal level.

To determine the spatial distribution of fractional ErAs coverage expected for given values of f and nanoparticle radius r , we assume that the spatial distribution of ErAs nanoparticles nucleated at the pn junction during growth is random and generate a simulated distribution of ErAs surface coverage by placing nanoparticles of radius r on the surface at random locations until the expected average fractional coverage f is reached. Figure 4(a) shows representative distributions of ErAs obtained for nanoparticle radii ranging from 4 nm to 10 nm. The simulated surface is then divided into $40\text{ nm} \times 40\text{ nm}$ areas and the fractional ErAs coverage in each such area is computed, yielding a spatially averaged value for fractional ErAs coverage analogous to that derived from the experimental SCM images. For both these simulations and the analysis of the SCM images described above, very similar results were obtained for averaging areas ranging from $30\text{ nm} \times 30\text{ nm}$ to $50\text{ nm} \times 50\text{ nm}$.

Figure 4(b) shows the statistical distributions of ErAs fractional surface coverage derived from the SCM images in Fig. 2, and computed for ErAs nanoparticle radii of 4 nm to 10 nm. The distribution derived from the SCM data corresponds closely to that expected for nanoparticle radii of 6-8 nm, with substantially poorer agreement observed for radii of 4 nm or 10 nm. From this comparison, we deduce that the average ErAs nanoparticle radius in our samples is 6-8 nm—consistent with prior studies of ErAs nanoparticle dimensions under similar growth conditions¹⁴ and considerably smaller than the resolution limit dictated by the probe tip size. This is possible due to differences in larger-scale spatial inhomogeneity that arise from very small nanoparticle sizes and variations thereof.

In summary, scanning capacitance microscopy has been used to characterize electronic properties and size distributions of ErAs nanoparticles embedded in GaAs pn junctions prepared via MBE growth. Analysis of bias-dependent SCM images combined with numerical modeling confirms that a high local density of ErAs nanoparticles can produce Fermi level pinning at the ErAs nanoparticle layer, while at lower local nanoparticle densities the effects of such pinning on car-

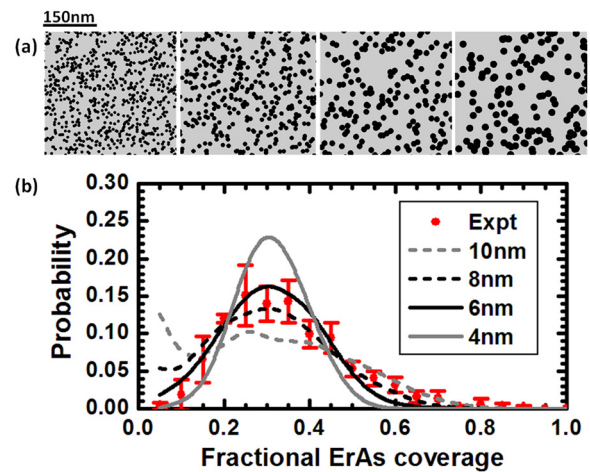


FIG. 4. (Color online) (a) Simulated distributions of ErAs coverage (dark areas) at the GaAs pn junction obtained by random placement of ErAs nanoparticles with radii of 4 nm, 6 nm, 8 nm, and 10 nm. For each distribution, the average fractional surface coverage is fixed at ~ 0.28 . (b) Normalized distributions of ErAs coverage fraction, averaged over $40\text{ nm} \times 40\text{ nm}$ areas, for simulated distributions of ErAs nanoparticles with radii of 4-10 nm, and as extracted from SCM images obtained at bias voltages from -2.0 V to 0.0 V.

rier modulation are reduced. A statistical analysis of spatial inhomogeneity in SCM images yields an average nanoparticle radius of 6-8 nm. Of particular note from a metrology perspective is that this value is smaller than the actual resolution limit in SCM that is dictated by probe tip size; such small particle dimensions can be deduced via analysis of the structure of larger-scale spatial inhomogeneity in local capacitance that arises from a particular nanoparticle size.

Part of this work was supported by NSF (DMR-0806755, DMR-1066430, and ECCS-0954732 CAREER), AFOSR YIP (FA9550-10-1-0182), ARO PECASE (W911NF-09-1-0434), and the Judson S. Swearingen Regents Chair in Engineering at the University of Texas at Austin.

- ¹J. M. O. Zide, A. Kleiman-Shwarscstein, N. C. Strandwitz, J. D. Zimmerman, T. Steenblock-Smith, A. C. Gossard, A. Forman, A. Ivanovskaya, and G. D. Stucky, *Appl. Phys. Lett.* **88**, 162103 (2006).
- ²G. Zeng, J. Bahk, J. E. Bowers, H. Lu, A. C. Gossard, S. L. Singer, A. Majumdar, Z. Bian, M. Zebarjadi, and A. Shakouri, *Appl. Phys. Lett.* **95**, 083503 (2009).
- ³J. M. O. Zide, D. Vashaee, Z. X. Bian, G. Zeng, J. E. Bowers, A. Shakouri, and A. C. Gossard, *Phys. Rev. B* **74**, 205335 (2006).
- ⁴H. Chen, W. J. Padilla, J. M. O. Zide, S. R. Bank, A. C. Gossard, A. J. Taylor, and R. D. Averitt, *Opt. Lett.* **32**, 1620 (2007).
- ⁵P. J. Hansen, Y. E. Strausser, A. N. Erickson, E. J. Tarsa, P. Kozodoy, E. G. Brazel, J. P. Ibbetson, U. Mishra, V. Narayanamurti, S. P. DenBaars, and J. S. Speck, *Appl. Phys. Lett.* **72**, 2247 (1998).
- ⁶K. V. Smith, E. T. Yu, J. M. Redwing, and K. S. Boutros, *Appl. Phys. Lett.* **75**, 2250 (1999).
- ⁷X. Zhou, E. T. Yu, D. Florescu, J. C. Ramer, D. S. Lee, and E. A. Armour, *Appl. Phys. Lett.* **85**, 407 (2004).
- ⁸C. Kadow, J. A. Johnson, K. Kolstad, J. P. Ibbetson, and A. C. Gossard, *J. Vac. Sci. Technol. B* **18**, 2197 (2000).
- ⁹H. P. Nair, A. M. Crook, and S. R. Bank, *Appl. Phys. Lett.* **96**, 222104 (2010).
- ¹⁰G. L. Snider, 1D Poisson/Schrödinger solver (University of Notre Dame, Notre Dame, IN, 1995).
- ¹¹T. Sands, C. J. Palmström, J. P. Harbison, V. G. Keramidis, N. Tabatabaie, T. L. Cheeks, R. Ramesh, and Y. Silberberg, *Mater. Sci. Rep.* **5**, 99 (1990).
- ¹²C. J. Palmström, T. L. Cheeks, H. L. Gilchrist, J. G. Zhu, C. B. Carter, B. J. Wilkens, and R. Martin, *J. Vac. Sci. Technol. A* **10**, 1946 (1992).
- ¹³K. T. Delaney, N. A. Spaldin, and C. G. Van de Walle, *Phys. Rev. B* **77**, 235117 (2008).
- ¹⁴B. D. Schultz and C. J. Palmström, *Phys. Rev. B* **73**, 241407 (2006).